# A PARAMETRIC MOVING TARGET DETECTOR FOR DISTRIBUTED MIMO RADAR IN NON-HOMOGENEOUS ENVIRONMENT

*Pu Wang*[*]*, Hongbin Li*[*]*, and Braham Himed*[‡]

[*] ECE DEPT, Stevens Institute of Technology, Hoboken, NJ 07030, USA
[‡] AFRL/RYMD, Dayton, OH 45433, USA

**ABSTRACT**

This paper addresses the problem of moving target detection (MTD) using a distributed multi-input multi-output (MIMO) radar in a non-homogeneous environment, where independent auto-regressive (AR) models are used to approximate the disturbance including clutter and noise as seen by different transmit-receive pairs. Following the proposed model, we develop a parametric generalized likelihood ratio test (PGLRT) for MTD with the distributed MIMO radar, which is referred to herein as MIMO-PGLRT. It is found that the resulting MIMO-PGLRT performs local adaptive subspace detection, non-coherent combining using local decision variables and a global threshold comparison. Asymptotic analysis of the MIMO-PGLRT statistic shows that the proposed detector can asymptotically achieve constant false alarm rate (CFAR). Numerical results are provided to verify our analysis and to compare the proposed MIMO-PGLRT with other MIMO MTD detectors.

***Index Terms***— Moving target detection, distributed multiple-input multiple-output (MIMO) radar, non-homogeneous clutter, auto-regressive process.

## 1. INTRODUCTION

A distributed multi-input multi-output (MIMO) radar employs widely separated antennas within the transmit and, respectively, receive aperture, and the transmit antennas probe a radar scene using multiple orthogonal waveforms which are separated at each receive antenna by matched filter processing [1–4]. A distributed MIMO radar allows one to exploit the *spatial or geometric diversity* to enhance target detection. In particular, radar targets often exhibit significant azimuth-selective backscattering with tens of dB of fluctuation in their radar cross section (RCS) [5]. As a result, it would be difficult for a traditional monostatic or bistatic radar to detect such targets, if the sensors are unfavorably located.

The spatial diversity of distributed MIMO radar was first discussed in [3] for stationary target detection and later extended in [4] for moving target detection. The focus of [3] was to establish the detection diversity gain, and the effect of clutter was ignored. Meanwhile, the effect of clutter was included in [4, 6] for moving target detection where it was shown that distributed MIMO radar systems can provide significant performance gain over traditional phased array radar systems. However, the clutter was assumed to be spatially *homogeneous*, i.e., the clutter covariance matrix is identical for all transmit-receive pairs and for all resolution cells. For adaptive detection, it was suggested to estimate the clutter covariance matrix using training data from adjacent resolution cells due to the homogeneous assumption.

Unlike most current efforts which assume a homogeneous clutter environment, we consider here the moving target detection (MTD) problem with a distributed MIMO radar in a *non-homogeneous* clutter environment, which arises from the multi-static transmit-receive configuration of the distributed MIMO radar. Specifically, for the same resolution cell, the clutter from different transmit-receiver antenna pairs may experience non-homogeneities in both speckle and texture due to azimuth-selective backscattering of the clutter sources. In addition, the clutter may also vary significantly across resolution cells in a neighborhood. To address this issue, a parametric auto-regressive (AR) model is proposed to describe the clutter speckle and texture variations. Using independent AR models for the disturbance including the clutter and noise associated with each transmit-receive pair, the parametric AR model is able to approximate non-homogeneous disturbance with a wide variety of Doppler spectrum.

Following the proposed model, we develop a parametric generalized likelihood ratio test (PGLRT) for MTD with the distributed MIMO radar. It is found that the resulting MIMO-PGLRT performs local adaptive subspace detection, non-coherent combining using local decision variables, and a global threshold comparison. The local detector first adaptively projects the test signal into two distinct subspaces: one is the orthogonal complement of a data matrix formed using the returned signal within a coherent processing interval (CPI) and the other is the orthogonal complement of a target-free data matrix. Then, it computes the energy of both projected test signals, followed by a comparison to obtain the local test variable. Asymptotic analysis is carried out, which shows that the MIMO-PGLRT is an asymptotically constant false alarm rate (CFAR) detector. Numerical results with both synthesized AR dataset and a general clutter model are provided for performance evaluation.

The remainder of the paper is organized as follows. A signal model is introduced in Section 2, where the parametric AR model for the non-homogeneous environment is defined. Following that, the MIMO-PGLRT is proposed and derived in closed form in Section 3. Simulation results are provided in Section 4 to show the effectiveness of the proposed detector. Finally, conclusions are drawn in Section 5.

## 2. SIGNAL MODEL

Consider a distributed MIMO radar system with $M$ transmit antenna elements and $N$ receive antenna elements. The transmit and receive antennas are assumed to be on stationary platforms. We use the standard assumption for MIMO radars that the $M$ transmit antennas probe a common area of interest using $M$ orthogonal waveforms [1–4, 6–11]. Pulsed transmission is employed as in standard

This work was supported in part by a subcontract with Dynetics, Inc. for research sponsored by the Air Force Research Laboratory (AFRL) under Contract FA8650-08-D-1303.

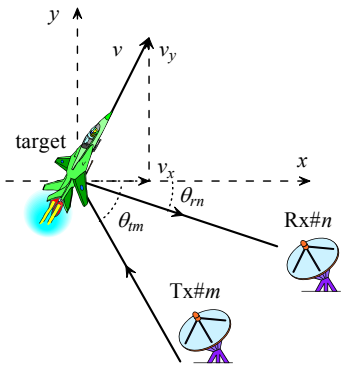


**Fig. 1**. Transmit-receive pair geometry of a distributed MIMO radar.

Doppler radars [5]. Each transmitter sends a succession of $K$ periodic pulses, i.e., $K$ repetitions of an orthogonal waveform, over a CPI. Each receiver employs a bank of $M$ matched filters corresponding to the $M$ orthogonal waveforms. The matched filter output is sampled at the pulse rate via *slow-time sampling*. Let $\mathbf{x}_{mn} \in \mathbb{C}^{K\times 1}$ denote the vector formed by the $K \times 1$ samples of the matched filter output (within a CPI) at the $n$-th receiver matched to the $m$-th transmitter. The problem of interest is to detect the presence/absence of a moving target in the cell of interest (test cell) using the observations $\{\mathbf{x}_{mn}\}$.

Specifically, the problem involves the following hypothesis testing [4, 6, 10, 11]:

$$\begin{aligned} H_0: &\quad \mathbf{x}_{mn} = \mathbf{c}_{mn} + \mathbf{w}_{mn}, \\ H_1: &\quad \mathbf{x}_{mn} = \alpha_{mn}\mathbf{s}(f_{mn}) + \mathbf{c}_{mn} + \mathbf{w}_{mn}, \\ &\qquad n = 1, \ldots, N; m = 1, \ldots, M, \end{aligned} \tag{1}$$

where $\mathbf{c}_{mn}$ denotes clutter, $\mathbf{w}_{mn}$ denotes noise, $\mathbf{s}(f_{mn})$ is the signal steering vector due to a Doppler frequency $f_{mn}$, and $\alpha_{mn}$ is the amplitude of the signal, which is determined by the radar cross section (RCS) of the target.

The Doppler frequency is due to the presence of a moving target, which is usually unknown at the receivers. The moving target has a velocity denoted by its $x$- and $y$-component $(v_x, v_y) \triangleq \mathbf{v}$, assuming a 2-dimensional (2-D) motion. This motion creates different Doppler frequencies for different transmit-receive antenna pairs. Using the geometry depicted in Figure 1, the normalized Doppler frequency $f_{mn}$ is given by [1, 4, 12]

$$f_{mn} = \frac{v_x T}{\lambda}\left(\cos\theta_{tm} + \cos\theta_{rn}\right) + \frac{v_y T}{\lambda}\left(\sin\theta_{tm} + \sin\theta_{rn}\right), \tag{2}$$

where $\lambda$ denotes the operating wavelength and $T$ is the pulse repetition interval (PRI). The signal steering vector, which is formed over the reception of $K$ coherent pulses, is given by

$$\mathbf{s}(f_{mn}) = \begin{bmatrix} 1 & e^{-j2\pi f_{mn}} & \ldots & e^{-j2\pi f_{mn}(K-1)} \end{bmatrix}^T. \tag{3}$$

The unknown signal amplitude $\alpha_{mn}$ is related to the target RCS. In general, it varies significantly with the aspect angle, due to the azimuth-selective backscattering [3–5]. As such, in our data model, $\alpha_{mn}$ is different for different transmit-receive antenna pairs.

The disturbance component $\mathbf{d}_{mn}$ includes the clutter $\mathbf{c}_{mn}$ and the noise $\mathbf{w}_{mn}$, i.e., $\mathbf{d}_{mn} = \mathbf{c}_{mn} + \mathbf{w}_{mn}$. Specifically, The clutter components $\mathbf{c}_{mn}$ contain reflections from stationary (e.g., ground, buildings) and slow moving objects (e.g., grass, forest) within the considered test cell, while the noise components $\mathbf{w}_{mn}$ are mainly from the thermal noise of the local receivers. We assume that the disturbance from any transmit-receive pair is a Gaussian-distributed vector with zero mean and covariance matrix $\mathbf{R}_{d,mn} = \mathbf{R}_{c,mn} + \mathbf{R}_{w,mn}$, where $\mathbf{R}_{c,mn}$ and $\mathbf{R}_{w,mn}$ denote the covariance matrices of the clutter and noise components, respectively. As a result, the disturbances for different transmit-receive pairs are essentially non-stationary due to distinct disturbance covariance matrices $\mathbf{R}_{d,mn}$, i.e., $\mathbf{R}_{d,mn} \neq \mathbf{R}_{d,m'n'}$, if $m \neq m'$ and $n \neq n'$ [6, 13, 14]. Moreover, for a given transmit-receive pair, the disturbances are also non-homogeneous for different range resolution cells and, therefore, the non-homogeneity takes place in the range domain and also across multiple transmit-receive pairs [13, 14].

In many situations, the disturbance can be modeled by an auto-regressive (AR) process with a relatively low order. For example, the AR order is between 2 and 5 for many radar echo modelings, while in active sonar environments it is usually chosen to be 8 [15–19]. Moreover, for a wide-sense stationary process with a given power spectral density (PSD), there exists an AR process such that, for each frequency, the error between the true PSD and the AR PSD is arbitrarily small [18]. Therefore, we propose to use independent AR processes to model the disturbances from multiple transmit-receive pairs:

$$d_{mn}(k) = -\sum_{p=1}^{P_{mn}} a_{mn}(p) d_{mn}(k-p) + \varepsilon_{mn}(k), k = 1, ..., K, \tag{4}$$

where the driving noise $\varepsilon_{mn}(k) \sim \mathcal{CN}(0, \sigma_{mn}^2)$ with $\sigma_{mn}^2$ denoting its variance, $a_{mn}(p), p = 1, \cdots, P_{mn}$, denotes the AR coefficient for the $(m, n)$-th transmit-receive pair, and $P_{mn}$ denotes the AR model order. Specifically, the speckle component of the disturbance may be described by the AR coefficients $a_{mn}(p)$ as well as the AR model order $P_{mn}$, while the texture components of the disturbance can be modeled by the variance of driving noise $\sigma_{mn}^2$. Overall, with $MN$ independent AR processes, it is possible to model the disturbances from the $MN$ transmit-receive pairs and provide a parametric approach to simulate the non-homogeneity of the disturbance in the distributed MIMO radar case

## 3. PARAMETRIC GLRT FOR THE MIMO-MTD

The MIMO-PGLRT detector is developed based upon the GLRT principle, which requires the maximum likelihood estimates of the unknown parameters $\alpha_{mn}, \sigma_{mn}^2$, and $\mathbf{a}_{mn} = [a_{mn}(1), \cdots, a_{mn}(P_{mn})]^T$. Due to statistical independence across multiple transmit-receive pairs, the MIMO-PGLRT takes the form of

$$\begin{aligned} T_{\text{MIMO-PGLR}} &= \frac{\max\limits_{\alpha_{mn},\mathbf{a}_{mn},\sigma_{mn}^2} \prod\limits_{m,n} f_1\left(\alpha_{mn}, \mathbf{a}_{mn}, \sigma_{mn}^2\right)}{\max\limits_{\mathbf{a}_{mn},\sigma_{mn}^2} \prod\limits_{m,n} f_0\left(\mathbf{a}_{mn}, \sigma_{mn}^2\right)} \\ &= \frac{\prod\limits_{m,n} \max\limits_{\alpha_{mn},\mathbf{a}_{mn},\sigma_{mn}^2} f_1\left(\alpha_{mn}, \mathbf{a}_{mn}, \sigma_{mn}^2\right)}{\prod\limits_{m,n} \max\limits_{\mathbf{a}_{mn},\sigma_{mn}^2} f_0\left(\mathbf{a}_{mn}, \sigma_{mn}^2\right)}. \end{aligned} \tag{5}$$

For the $(m, n)$-th transmit-receive pair, the likelihood function of $\mathbf{x}_{mn}$ can be asymptotically expressed as

$$f_i(\mathbf{x}_{mn}) = \frac{1}{(\pi\sigma_{mn}^2)^{(K-P_{mn})}} \exp\left\{-\frac{1}{\sigma_{mn}^2} \sum_{k=P_{mn}+1}^{K} |\varepsilon_{mn}(k)|^2\right\}, \tag{6}$$

where $i = \{0, 1\}$ denotes $H_0$ and $H_1$, respectively. Let

$$\mathbf{x}_{mn} = [x_{mn}(P_{mn}+1), x_{mn}(P_{mn}+2), \cdots, x_{mn}(K)]^T,$$
$$\mathbf{s}_{mn} = [s_{mn}(P_{mn}+1), s_{mn}(P_{mn}+2), \cdots, s_{mn}(K)]^T,$$

and define the $P_{mn} \times 1$ regressive vectors of $x_{mn}(k)$ and $s_{mn}(k)$

$$\mathbf{y}_{mn}(k) = [x_{mn}(k-1), x_{mn}(k-2), \cdots, x_{mn}(k-P_{mn})]^T,$$
$$\mathbf{t}_{mn}(k) = [s_{mn}(k-1), s_{mn}(k-2), \cdots, s_{mn}(k-P_{mn})]^T.$$

The likelihood function can be expressed as

$$f_0(\mathbf{x}_{mn}) = \frac{e^{-\frac{1}{\sigma^2_{mn}}\sum_{k=P_{mn}+1}^{K}\left|x_{mn}(k)+\mathbf{y}^T_{mn}(k)\mathbf{a}_{m,n}\right|^2}}{(\pi\sigma^2_{mn})^{(K-P_{mn})}},$$
$$f_1(\mathbf{x}_{mn}) = \frac{e^{-\frac{1}{\sigma^2_{mn}}\sum_{k}\left|\left(x_{mn}(k)+\mathbf{y}^T_{mn}(k)\mathbf{a}_{mn}\right)-\alpha_{mn}\left(s_{mn}(k)+\mathbf{t}^T_{mn}(k)\mathbf{a}_{mn}\right)\right|^2}}{(\pi\sigma^2_{mn})^{(K-P_{mn})}}. \tag{7}$$

Further define the following $(K - P_{mn}) \times P_{mn}$ matrices,

$$\mathbf{Y}_{mn} = [\mathbf{y}_{mn}(P_{mn}+1), \mathbf{y}_{mn}(P_{mn}+2), \cdots, \mathbf{y}_{mn}(K)]^T,$$
$$\mathbf{T}_{mn} = [\mathbf{t}_{mn}(P_{mn}+1), \mathbf{t}_{mn}(P_{mn}+2), \cdots, \mathbf{t}_{mn}(K)]^T. \tag{8}$$

The above likelihood function for the $(m, n)$-th transmit-receive pair can be simplified as

$$f_0(\mathbf{x}_{mn}) = \frac{e^{-\frac{1}{\sigma^2_{mn}}\|\mathbf{x}_{mn}+\mathbf{Y}_{mn}\mathbf{a}_{mn}\|^2}}{(\pi\sigma^2_{mn})^{(K-P_{mn})}},$$
$$f_1(\mathbf{x}_{mn}) = \frac{e^{-\frac{1}{\sigma^2_{mn}}\|[\mathbf{x}_{mn}+\mathbf{Y}_{mn}\mathbf{a}_{mn}]-\alpha_{mn}[\mathbf{s}_{mn}+\mathbf{T}_{mn}\mathbf{a}_{mn}]\|^2}}{(\pi\sigma^2_{mn})^{(K-P_{mn})}}. \tag{9}$$

It is seen that $\tilde{\mathbf{x}}_{mn} \triangleq \mathbf{x}_{mn}+\mathbf{Y}_{mn}\mathbf{a}_{mn}$ and $\tilde{\mathbf{s}}_{mn} \triangleq \mathbf{s}_{mn}+\mathbf{T}_{mn}\mathbf{a}_{mn}$ are the temporally whitened received signal and steering vector, respectively.

### 3.1. Maximum Likelihood Estimation under $H_1$

Due to the statistical independence across different transmit-receive pairs, we can first find the ML estimate of the variance of the driving noise of the AR model as

$$\hat{\sigma}^2_{mn} = \frac{1}{K-P_{mn}}\|[\mathbf{x}_{mn}+\mathbf{Y}_{mn}] - \alpha_{mn}[\mathbf{s}_{mn}+\mathbf{T}_{mn}\mathbf{a}_{mn}]\|^2. \tag{10}$$

The ML estimate of the amplitude $\alpha_{mn}$ is obtained equivalently by minimizing the term

$$\|[\mathbf{x}_{mn}+\mathbf{Y}_{mn}\mathbf{a}_{mn}] - \alpha_{mn}[\mathbf{s}_{mn}+\mathbf{T}_{mn}\mathbf{a}_{mn}]\|^2 \tag{11}$$

with respect to (w.r.t.) $\alpha_{mn}$, yielding

$$\hat{\alpha}_{mn} = \frac{(\mathbf{s}_{mn}+\mathbf{T}_{mn}\mathbf{a}_{mn})^H(\mathbf{x}_{mn}+\mathbf{Y}_{mn}\mathbf{a}_{mn})}{(\mathbf{s}_{mn}+\mathbf{T}_{mn}\mathbf{a}_{mn})^H(\mathbf{s}_{mn}+\mathbf{T}_{mn}\mathbf{a}_{mn})}. \tag{12}$$

As a result, the likelihood function is shown to be

$$f_1\left(\mathbf{x}_{mn}\left|\hat{\alpha}_{mn}, \mathbf{a}_{mn}, \hat{\sigma}^2_{mn}\right.\right) = \left[\frac{K-P_{mn}}{(e\pi)(\mathbf{x}_{mn}+\mathbf{Y}_{mn}\mathbf{a}_{mn})^H\mathbf{P}^{\perp}_{mn}(\mathbf{x}_{mn}+\mathbf{Y}_{mn}\mathbf{a}_{mn})}\right]^{K-P_{mn}} \tag{13}$$

where

$$\mathbf{P}^{\perp}_{mn} = \mathbf{I} - \frac{(\mathbf{s}_{mn}+\mathbf{T}_{mn}\mathbf{a}_{mn})(\mathbf{s}_{mn}+\mathbf{T}_{mn}\mathbf{a}_{mn})^H}{(\mathbf{s}_{mn}+\mathbf{T}_{mn}\mathbf{a}_{mn})^H(\mathbf{s}_{mn}+\mathbf{T}_{mn}\mathbf{a}_{mn})} = \mathbf{I} - \frac{\tilde{\mathbf{s}}_{mn}\tilde{\mathbf{s}}^H_{mn}}{\tilde{\mathbf{s}}^H_{mn}\tilde{\mathbf{s}}_{mn}}. \tag{14}$$

Next, we show that the projection matrix $\mathbf{P}^{\perp}_{mn}$ is independent of the AR coefficient $\mathbf{a}_{mn}$. First, note that [15, 17]

$$\begin{aligned}\tilde{s}_{mn}(k+1) =& s_{mn}(k+1) + \mathbf{t}^T_{mn}(k+1)\mathbf{a}_{mn}\\ =& s_{mn}(k+1) + \sum_{p=1}^{P_{mn}} a_{mn}(p)s_{mn}(k+1-p)\\ =& s_{mn}(k)e^{j2\pi f_{mn}} + \sum_{p=1}^{P_{mn}} a_{mn}(p)s_{mn}(k-p)e^{j2\pi f_{mn}}\\ =& e^{j2\pi f_{mn}}\tilde{s}_{mn}(k),\end{aligned} \tag{15}$$

due to the definition

$$s_{mn}(k) = e^{j2\pi(k-1)f_{mn}} = s_{mn}(k+1)e^{-j2\pi f_{mn}} \tag{16}$$

Therefore,

$$\begin{aligned}\tilde{\mathbf{s}}_{mn} &= \tilde{s}_{mn}(P_{mn}+1)\left[1, e^{j2\pi f_{mn}}, \cdots, e^{j2\pi(K-P_{mn}-1)f_{mn}}\right]^T\\ &\triangleq \tilde{s}_{mn}(P_{mn}+1)\boldsymbol{\psi}_{mn},\end{aligned} \tag{17}$$

which updates the projection matrix $\mathbf{P}^{\perp}_{mn}$ as

$$\begin{aligned}\mathbf{P}^{\perp}_{mn} &= \mathbf{I} - \frac{|\tilde{s}_{mn}(P_{mn}+1)|^2\boldsymbol{\psi}_{mn}\boldsymbol{\psi}^H_{mn}}{|\tilde{s}_{mn}(P_{mn}+1)|^2\boldsymbol{\psi}^H_{mn}\boldsymbol{\psi}_{mn}}\\ &= \mathbf{I} - \frac{\boldsymbol{\psi}_{mn}\boldsymbol{\psi}^H_{mn}}{\boldsymbol{\psi}^H_{mn}\boldsymbol{\psi}_{mn}}\\ &\triangleq \mathbf{P}^{\perp}_{\boldsymbol{\psi}_{mn}}\end{aligned} \tag{18}$$

Clearly, $\mathbf{P}^{\perp}_{mn}$ is equivalent to $\mathbf{P}^{\perp}_{\boldsymbol{\psi}_{mn}}$ and it is not a function of $\mathbf{a}_{mn}$.

With this observation, the ML estimate of $\mathbf{a}_{mn}$ under $H_1$ minimizes the term

$$(\mathbf{x}_{mn}+\mathbf{Y}_{mn}\mathbf{a}_{mn})^H\mathbf{P}^{\perp}_{\boldsymbol{\psi}_{mn}}(\mathbf{x}_{mn}+\mathbf{Y}_{mn}\mathbf{a}_{mn}) \tag{19}$$

and the solution is

$$\hat{\mathbf{a}}_{mn,1} = -\left(\mathbf{Y}^H_{mn}\mathbf{P}^{\perp}_{\psi_{mn}}\mathbf{Y}_{mn}\right)^{-1}\mathbf{Y}^H_{mn}\mathbf{P}^{\perp}_{\psi_{mn}}\mathbf{x}_{mn}. \tag{20}$$

The likelihood function is simplified to

$$f_1\left(\mathbf{x}_{mn}\left|\hat{\alpha}_{mn}, \hat{\mathbf{a}}_{mn,1}, \hat{\sigma}^2_{mn}\right.\right) = \left[\frac{K-P_{mn}}{(e\pi)(\mathbf{x}_{mn}+\mathbf{Y}_{mn}\hat{\mathbf{a}}_{mn,1})^H\mathbf{P}^{\perp}_{\boldsymbol{\psi}_{mn}}(\mathbf{x}_{mn}+\mathbf{Y}_{mn}\hat{\mathbf{a}}_{mn,1})}\right]^{K-P_{mn}}. \tag{21}$$

### 3.2. Maximum Likelihood Estimation under $H_0$

Similarly, we can show that the ML estimates of $\sigma^2_{mn}$ and $\mathbf{a}_{mn}$ can be obtained as

$$\hat{\sigma}^2_{mn} = \frac{1}{K-P_{mn}}\|\mathbf{x}_{mn}+\mathbf{Y}_{mn}\mathbf{a}_{mn}\|^2, \tag{22}$$

$$\hat{\mathbf{a}}_{mn,0} = -\left(\mathbf{Y}^H_{mn}\mathbf{Y}_{mn}\right)^{-1}\mathbf{Y}^H_{mn}\mathbf{x}_{mn}, \tag{23}$$

which gives the likelihood function under $H_0$

$$f_0\left(\mathbf{x}_{mn}\left|\hat{\mathbf{a}}_{mn,0},\hat{\sigma}^2_{mn}\right.\right)=\left[\frac{K-P_{mn}}{(e\pi)\left\|\mathbf{x}_{mn}+\mathbf{Y}_{mn}\hat{\mathbf{a}}_{mn,0}\right\|^2}\right]^{K-P_{mn}}. \tag{24}$$

### 3.3. MIMO-PGLRT Statistic

With the above results, we show that the test statistic of the MIMO-PGLRT takes the form

$$T=\prod_{m,n}\left[\frac{\left\|\mathbf{x}_{mn}+\mathbf{Y}_{mn}\hat{\mathbf{a}}_{mn,0}\right\|^2}{\left(\mathbf{x}_{mn}+\mathbf{Y}_{mn}\hat{\mathbf{a}}_{mn,1}\right)^H\mathbf{P}^{\perp}_{\boldsymbol{\psi}_{mn}}\left(\mathbf{x}_{mn}+\mathbf{Y}_{mn}\hat{\mathbf{a}}_{mn,1}\right)}\right]^{K-P_{mn}} \tag{25}$$

With the ML estimates of $\mathbf{a}_{mn}$ under both $H_0$ and $H_1$, the test statistic can be further simplified by noting that

$$\begin{aligned}&\frac{\left(\mathbf{x}_{mn}+\mathbf{Y}_{mn}\hat{\mathbf{a}}_{mn,0}\right)^H\left(\mathbf{x}_{mn}+\mathbf{Y}_{mn}\hat{\mathbf{a}}_{mn,0}\right)}{\left(\mathbf{x}_{mn}+\mathbf{Y}_{mn}\hat{\mathbf{a}}_{mn,1}\right)^H\mathbf{P}^{\perp}_{\boldsymbol{\psi}_{mn}}\left(\mathbf{x}_{mn}+\mathbf{Y}_{mn}\hat{\mathbf{a}}_{mn,1}\right)}\\&=\frac{\mathbf{x}^H_{mn}\mathbf{P}^{\perp}_{\mathbf{Y}_{mn}}\mathbf{x}_{mn}}{\mathbf{x}^H_{mn}\mathbf{P}^{\perp}_{\left[\mathbf{P}^{\perp}_{\boldsymbol{\psi}_{mn}}\mathbf{Y}_{mn}\right]}\mathbf{x}_{mn}}\end{aligned}$$

where

$$\mathbf{P}^{\perp}_{\mathbf{Y}_{mn}}=\mathbf{I}-\mathbf{Y}_{mn}\left(\mathbf{Y}^H_{mn}\mathbf{Y}_{mn}\right)^{-1}\mathbf{Y}^H_{mn}, \tag{26}$$

$$\mathbf{P}^{\perp}_{\left[\mathbf{P}^{\perp}_{\boldsymbol{\psi}_{mn}}\mathbf{Y}_{mn}\right]}=\mathbf{I}-\mathbf{P}^{\perp}_{\boldsymbol{\psi}_{mn}}\mathbf{Y}_{mn}\left(\mathbf{Y}^H_{mn}\mathbf{P}^{\perp}_{\boldsymbol{\psi}_{mn}}\mathbf{Y}_{mn}\right)^{-1}\mathbf{Y}^H_{mn}\mathbf{P}^{\perp}_{\boldsymbol{\psi}_{mn}}. \tag{27}$$

Finally, the MIMO-PGLRT takes the form of

$$T_{\text{MIMO-PGLR}}=\prod_{m,n}\left[\frac{\mathbf{x}^H_{mn}\mathbf{P}^{\perp}_{\mathbf{Y}_{mn}}\mathbf{x}_{mn}}{\mathbf{x}^H_{mn}\mathbf{P}^{\perp}_{[\mathbf{P}^{\perp}_{\boldsymbol{\psi}_{mn}}\mathbf{Y}_{mn}]}\mathbf{x}_{mn}}\right]^{K-P_{mn}}\underset{H_0}{\overset{H_1}{\gtrless}}\tau_{\text{MIMO-PGLR}}, \tag{28}$$

where $\tau_{\text{MIMO-PGLR}}$ is a threshold subject to a selected probability of false alarm. It is found that the resulting MIMO-PGLRT performs local adaptive subspace detection, non-coherent combining using local decision variables, and a global threshold comparison. The local detector first adaptively projects the test signal into two distinct subspaces: one is the orthogonal complement of a data matrix formed using the returned signal within a CPI and the other is the orthogonal complement of a target-free data matrix. Then, it computes the energy of both projected test signals, followed by a comparison to obtain the local test variable.

In the following, the asymptotic distribution of the MIMO-PGLRT statistic is derived.

### 3.4. Asymptotic Distribution of the MIMO-PGLRT Statistic

The exact distribution of the MIMO-PGLRT under both hypotheses is difficult to analyze. Instead, the asymptotic distribution of the GLRT is given by

$$T_{\text{MIMO - PGLR}}\overset{a}{\sim}\begin{cases}\chi^2_{2MN}\\ \chi^2_{2MN}\left(\xi\right)\end{cases} \tag{29}$$

In other words, the MIMO-PGLRT statistic is, under $H_0$, distributed according to the central Chi-square distribution with degrees of freedom $2MN$, whereas it is distributed as a non-central Chi-square distribution with degrees of freedom $2MN$ and non-centrality parameter $\xi$:

$$\xi=2\sum_{m,n}\frac{\left|\alpha_{mn}\right|^2}{\sigma^2_{mn}}\tilde{\mathbf{s}}^H_{mn}\tilde{\mathbf{s}}_{mn} \tag{30}$$

where $\tilde{\mathbf{s}}_{m,n}=\mathbf{s}_{m,n}+\mathbf{T}_{m,n}\mathbf{a}_{m,n}$ denotes the whitened steering vector by using the true AR coefficient $\mathbf{a}_{mn}$.

From the distributions of the MIMO-PGLRT statistic, we can analytically compute the probability of detection and the probability of false alarm. Meanwhile, we can verify that the distribution of the MIMO-PGLRT statistic under $H_0$ is independent of the disturbance parameters including the AR coefficient $\mathbf{a}_{mn}$ and the driving noise variance $\sigma^2_{mn}$, and hence, the MIMO-PGLRT detector asymptotically achieves CFAR.

### 3.5. Sample Covariance Matrix-Based Detector

An existing detector for the MTD with distributed MIMO radar is the sample covariance matrix (SCM)- based detector [4, 6]:

$$T_{\text{SCM}}=\sum_{m,n}\frac{\left|\mathbf{a}^H_{mn}\hat{\mathbf{C}}^{-1}_{mn}\mathbf{x}_{mn}\right|^2}{\mathbf{a}^H_{mn}\hat{\mathbf{C}}^{-1}_{mn}\mathbf{a}_{mn}}\underset{H_0}{\overset{H_1}{\gtrless}}\tau_{\text{SCM}}, \tag{31}$$

where $\tau_{\text{SCM}}$ is a threshold for a given probability of false alarm, and $\hat{\mathbf{C}}_{mn}$ is the sample covariance matrix computed from $K_t$ *homogeneous* training signals $\mathbf{x}_{mn,k_t}\in\mathbb{C}^{K\times 1}$, $k_t=1,2,\cdots,K_t$, for the $(m,n)$-th transmit-receive pair:

$$\hat{\mathbf{C}}_{mn}=\frac{1}{K_t}\sum_{k_t=1}^{K_t}\mathbf{x}_{mn,k_t}\mathbf{x}^H_{mn,k_t}. \tag{32}$$

To ensure that the sample covariance matrix is full rank, $K_t>K$ range training signals are required for each transmit-receive pair. In general, $K_t=2K$ training signals are needed for a reasonable performance. As such, the SCM detector (31) requires about $2KMN$ training signals in total, which may be difficult to fulfill in a non-homogeneous environment. Compared with the SCM detector, the proposed MIMO-PGLRT requires no range training signals and estimates the parameters associated with disturbance adaptively from the received test signal. It is also computationally simpler to implement the MIMO-PGLRT than the SCM detector since the SCM requires the estimation and inversion of the sample covariance matrix for each transmit-receive pair.

## 4. NUMERICAL EVALUATION

In this section, numerical results are presented to verify the asymptotic analysis and to compare the performance of the proposed MIMO-PGLRT with that of the SCM detector (31) in non-homogeneous clutter environments. The distributed MIMO configuration is shown in Fig. 2, which consists of two transmitters at $0^\circ$ and $65^\circ$ relative to the target and two receivers at $-30^\circ$ and $40^\circ$. It is noted that the configuration is the same as the one used in [4] and [6]. The pulse repetition frequency is 500 Hz, the carrier frequency is 1 GHz, the target velocity is 108 km/h, and the number of pulses within a CPI is $K=32$. The above parameters lead to a normalized target Doppler frequency of $|\mathbf{v}|T_{\text{PRI}}/\lambda=0.2$ in (2).

We examine the detection performance of the MIMO-PGLRT and the SCM detector in terms of the receiver operating characteristic (ROC). Specifically, we simulate average detection performance averaged over the target moving direction. We consider two

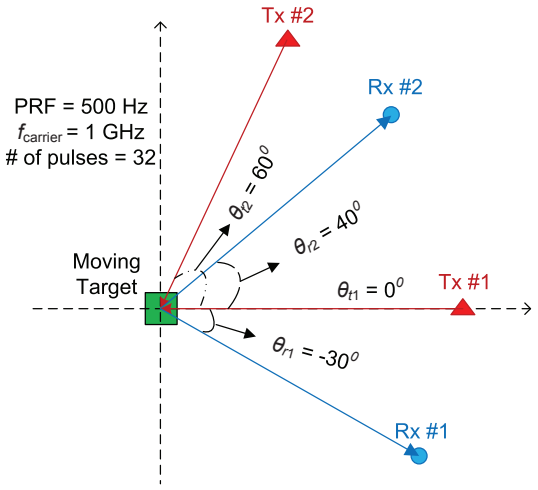


**Fig. 2**. Distributed MIMO radar configuration used in simulation.

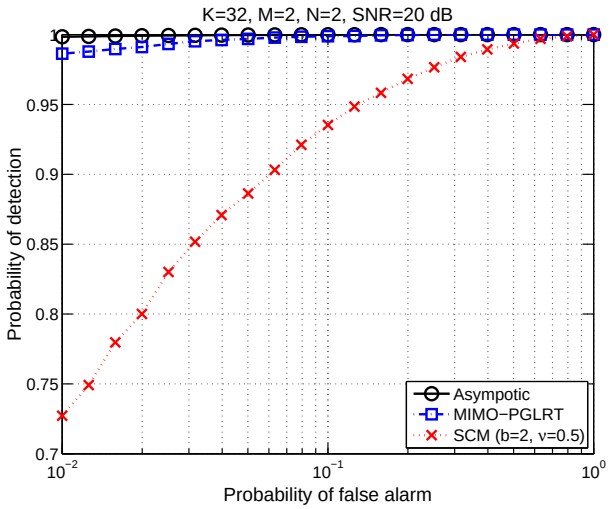


**Fig. 3**. Receiver-operating-characteristic (ROC) curves for the MIMO-PGLRT and the SCM detectors with a random target moving direction and non-fluctuating target amplitudes.

different target characteristic cases. In Case A, the moving direction is randomly chosen according to a uniform distribution over the range $[-180^\circ, 180^\circ]$ during each simulation trial, while the target amplitude is kept constant for all transmit-receive pairs, i.e., *non-fluctuating* target amplitudes. Case B considers not only a random target moving direction as in Case A but random (*fluctuating*) target amplitude as well. Specifically, $\alpha_{m,n}$ are generated as complex Gaussian random variables with zero mean and variance $\sigma^2_{\alpha_{m,n}} = 1$.

### 4.1. Synthesized AR Dataset

In the first example, we examine the MIMO-PGLRT and the SCM detectors with the synthesized AR dataset, where the disturbances from transmit-receive pairs are generated using independent AR processes. Here, we consider the following AR models for the disturbances from all four transmit-receive pairs: (1) $P_{11} = 3, \sigma^2_{11} = 1, \mathbf{a}_{11} = [-0.46 - j0.21, -0.17 - j0.2, 0.01 - j0.06]^T$; (2) $P_{12} = 2, \sigma^2_{12} = 0.5, \mathbf{a}_{12} = [-0.32 + j0.24, -0.33 + j0.22]^T$; (3) $P_{21} = 1, \sigma^2_{21} = 2, \mathbf{a}_{21} = [-0.1]^T$; (4) $P_{22} = 2, \sigma^2_{22} = 0.8, \mathbf{a}_{22} = [-0.34 - j0.31, -0.2 + j0.10]^T$. For the SCM detector, the $K_t = 2K$ training signals for each transmit-receive pair are generated using a compound-Gaussian model where the *texture* component is used to capture the power variation across range resolution cells. Particularly, we use the typical compound-Gaussian model: a $K$-distributed clutter with a scaling factor 0.5 and a shape factor 2. Otherwise, for each transmit-receive pair, the training signals share the same *speckle* component as the disturbance in the test signal.

Fig. 3 shows the ROC for both the MIMO-PGLRT and the SCM detector of Case A with a random moving direction and non-fluctuating target amplitude. Also included in the figure is the asymptotic performance derived in Section 3.4. The results show that the MIMO-PGLRT, without any range training signals, outperforms the SCM detector which suffers from the power-varying training signals. It is also suggested that, with only $K = 32$ temporal (Doppler) samples, the simulated performance of the MIMO-PGLRT is quite close to the derived asymptotic performance.

Fig. 4 shows the ROC curves for both the MIMO-PGLRT and the SCM detector of Case B with a random moving direction and fluctuating target amplitude. It confirms again that, in the case of fluctuating target amplitude, the MIMO-PGLRT still performs better than the SCM detector which uses power-varying training signals. When comparing Fig. 4 and Fig. 3 with non-fluctuating amplitudes, a performance loss is observed for both detectors.

### 4.2. General Clutter Model

The above results are all based upon the synthesized AR dataset. In the following, we consider a practical clutter model which has widely been used to model the clutter Doppler characteristics and is not necessarily an AR process [5, 6]. As such, we are able to evaluate the performance of the MIMO-PGLRT in the case of model mismatch.

The clutter temporal correlation function is expressed as [5, 6]

$$\Phi(\tau) = P_c e^{-8\pi^2 \tau^2 \frac{\delta_v^2}{\lambda^2}} \triangleq P_c \phi(\tau). \tag{33}$$

where $P_c$ is the clutter power, and $\delta_v$ is the root mean-square (RMS) of the clutter velocity. The covariance matrix $\mathbf{C}(P_c)$ is obtained by sampling the above temporal correlation function at $\tau = kT_{\text{PRF}}, k = 0, \cdots, K-1$ [5, 6]:

$$\mathbf{C}(P_c) = P_c \begin{pmatrix} \rho(0) & \rho(1) & \cdots & \rho(K-1) \\ \rho(1) & \rho(0) & \cdots & \vdots \\ \vdots & \vdots & \ddots & \rho(1) \\ \rho(K-1) & \cdots & \rho(1) & \rho(0) \end{pmatrix} \tag{34}$$

where $\rho(k) = \phi(kT_{\text{PRF}})$. In addition to the clutter, the noise is assumed to be spatially and temporally white Gaussian with zero mean and variance $\sigma^2_{w,mn}$. To account for the non-homogeneous nature of the clutter power caused by azimuth-selective backscattering, the range training signals are modeled using the compound-Gaussian model, where the texture component is assumed to be Gamma distributed with a scaling factor 0.5 and a shape factor 2, while the speckle component is assumed to be the same as the disturbance including the clutter and noise in the test signal. The target is simulated according to Case B with a random target moving direction

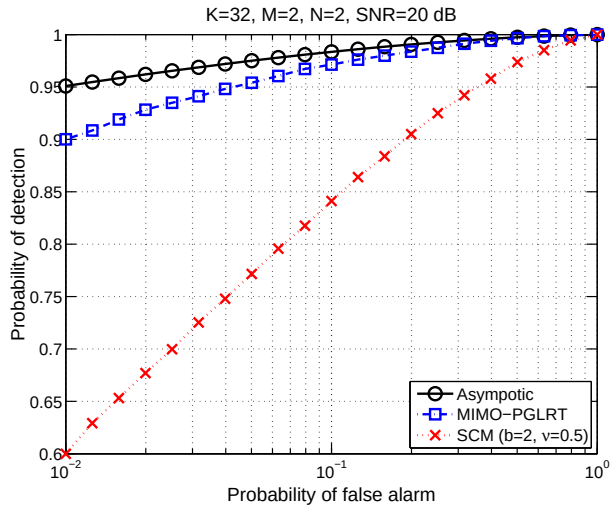


**Fig. 4**. ROC curves for the MIMO-PGLRT and the SCM detectors with a random target moving direction and fluctuating target amplitudes.

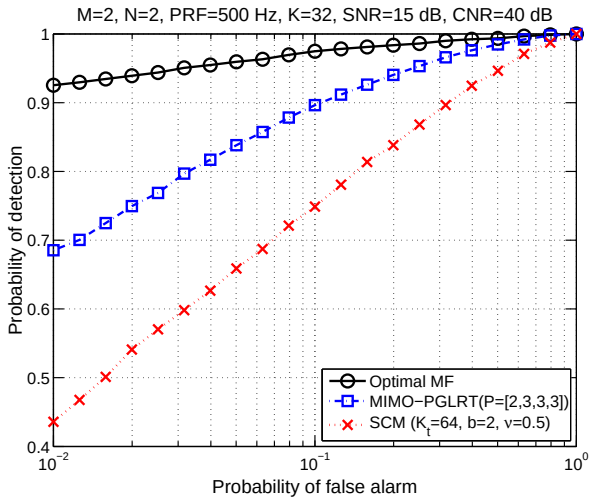


**Fig. 5**. ROC curves for the MIMO-PGLRT and the SCM detectors in the general clutter model with a random target moving direction and fluctuating target amplitudes.

and fluctuating target amplitudes. Accordingly, the signal-to-noise ratio (SNR) is defined as

$$\text{SNR} = \frac{KMN \sum\limits_{m,n} \sigma^2_{\alpha_{m,n}}}{\sum\limits_{m,n} \sigma^2_{w,mn}}, \tag{35}$$

and the clutter-to-noise ratio (CNR) is defined as

$$\text{CNR} = \frac{KMN \sum_{m,n} P_c(m,n)}{\sum\limits_{m,n} \sigma^2_{w,mn}}. \tag{36}$$

Overall, the RMS values of the clutter velocity are selected to be different for all four transmit-receive pairs: $\delta_v = [0.5, 2.5, 1.5, 1.5]$ m/s and the power $P_c$ for all four transmit-receiver pairs are randomly selected (and hence different) and normalized with respect to the CNR.

The simulated results are shown in Fig. 5 with the general clutter model. It is seen that, with AR model orders $P_{mn} = [2, 3, 3, 3]$, the MIMO-PGLRT is able to handle the disturbance generated according to the general clutter model and provides better detection performance than the SCM detector which again suffers from the $K_t = 64$ power-varying range training signals for each transmit-receive pair. In summary, the parametric AR model provides an efficient way to model the disturbance and the MIMO-PGLRT is capable of dealing with non-homogeneous disturbances by exploiting the AR structure of the disturbance.

## 5. CONCLUSION

This paper introduced a parametric auto-regressive model for the disturbance received by a distributed MIMO radar. With independent AR processes, the proposed signal model is able to describe the non-homogeneity among different transmit-receive pairs, due to azimuth-selective backscattering of the clutter scatters. A parametric GLRT detector, which is referred to as MIMO-PGLRT, is proposed to exploit the inherent AR structure of the disturbance. An asymptotic analysis of the MIMO-PGLRT statistic is also derived and our results suggest that the MIMO-PGLRT asymptotically achieves a CFAR feature. Simulation results with both synthesized AR dataset and a general clutter model confirm that the MIMO-PGLRT is able to handle the non-homogeneous nature of the environment seen in distributed MIMO radar systems, and the MIMO-PGLRT outperforms sample-covariance-matrix based detectors which suffer with the non-homogeneous training signals.

## 6. REFERENCES

[1] B. Himed, H. Bascom, J. Clancy, and M. C. Wicks, "Tomography of moving target (TMT)," in *Sensors, Systems, and Next-Generation Satellites V*, Hiroyuki Fujisada, Joan B. Lurie, and Konradin Weber, Eds., vol. 4540, pp. 608–619. Proceedings of SPIE, 2001.

[2] M. C. Wicks, B. Himed, L. J. E. Bracken, H. Bascom, and J. Clancy, "Ultra narrow band adaptive tomographic radar," in *Proceedings of 2005 First IEEE International Workshop on Computational Advances in Multi-Sensor Adaptive Processing*, December 13-15 2005, pp. 36–39.

[3] E. Fishler, A. M. Haimovich, R. S. Blum, L. J. Cimini, Jr., D. Chizhik, and R. A. Valenzuela, "Spatial diversity in radars – models and detection performance," *IEEE Transactions on Signal Processing*, vol. 54, no. 3, pp. 823–838, March 2006.

[4] A. M. Haimovich, R. S. Blum, and L. J. Cimini, "MIMO radar with widely separated antennas," *IEEE Signal Processing Magazine*, vol. 25, no. 1, pp. 116–129, January 2008.

[5] M. I. Skolnik, *Introduction to Radar Systems*, McGraw-Hill, New York, NY, 3 edition, 2001.

[6] Q. He, N. H. Lehmann, R. S. Blum, and A. M. Haimovich, "MIMO radar moving target detection in homogeneous clutter," *IEEE Transactions on Aerospace and Electronic Systems*, vol. 46, no. 3, pp. 1290–1301, July 2010.

[7] N. A. Goodman, "Optimum and decentralized detection for multistatic airborne radar," *IEEE Transactions on Aerospace*

*and Electronic Systems*, vol. 43, no. 2, pp. 806–813, April 2007.

[8] A. De Maio and M. Lops, "Design principles of MIMO radar detectors," *IEEE Transactions on Aerospace and Electronic Systems*, vol. 43, no. 3, pp. 886–898, July 2007.

[9] T. Aittomaki and V. Koivunen, "Performance of MIMO radar with angular diversity under Swerling scattering models," *IEEE Journal of Selected Topics in Signal Processing*, vol. 4, no. 1, pp. 101–114, February 2010.

[10] C. Y. Chong, F. Pascal, J.-P. Ovarlez, and M. Lesturgie, "MIMO radar detection in non-Gaussian and heterogeneous clutter," *IEEE Journal of Selected Topics in Signal Processing*, vol. 4, no. 1, pp. 115–126, February 2010.

[11] Q. He, R. Blum, H. Godrich, and A. Haimovich, "Target velocity estimation and antenna placement for MIMO radar with widely separated antennas," *IEEE Journal of Selected Topics in Signal Processing*, vol. 4, no. 1, pp. 79–100, February 2010.

[12] N. J. Willis, *Bistatic Radar*, SciTech Publishing, 2 edition, 2005.

[13] P. Wang, H. Li, and B. Himed, "Moving target estimation using distributed MIMO radar in non-homogeneous clutter," in *Proceedings of the International Radar Symposium (IRS 2010)*, Vilnius, Lithuania, 16-18 June 2010.

[14] P. Wang, H. Li, and B. Himed, "Moving target detection using distributed MIMO radar in clutter with non-homogeneous power," *IEEE Transactions on Signal Processing*, to appear 2011.

[15] A. Sheikhi, M.M. Nayebi, and M.R. Aref, "Adaptive detection algorithm for radar signals in autoregressive interference," *IEE Proc.-Radar Sonar Navig.*, vol. 145, no. 5, pp. 309–314, 1998.

[16] J. R. Román, M. Rangaswamy, D. W. Davis, Q. Zhang, B. Himed, and J. H. Michels, "Parametric adaptive matched filter for airborne radar applications," *IEEE Transactions on Aerospace and Electronic Systems*, vol. 36, no. 2, pp. 677–692, April 2000.

[17] G. Alfano, A. De Maio, and A. Farina, "Model-based adaptive detection of range-spread targets," *IEE Proc.-Radar Sonar Navig.*, vol. 151, no. 1, pp. 2–10, February 2004.

[18] S. Haykin and A. Steinhardt, *Radar Detection and Estimation*, Wiley, 1992.

[19] S. M. Kay, *Modern Spectral Estimation: Theory and Application*, Prentice Hall, Englewood Cliffs, NJ, 1988.